Postprint of: Wasilczuk F., Flaszyński P., Doerffer P., Marugi K., Borzęcki T., The Application of Fluidic Sealing in Shrouded Gas Turbine Blades, JOURNAL OF TURBOMACHINERY-TRANSACTIONS OF THE ASME, Vol. 146, iss. 1 (2024), 015001, DOI: 10.1115/1.4064045

https://asmedigitalcollection.asme.org/turbomachinery/article-abstract/146/1/015001/1170048/The-Application-of-Fluidic-Sealing-in-Shrouded-Gas?redirectedFrom=fulltext

The Application of Fluidic Sealing in Shrouded Gas Turbine Blades

Filip Wasilczuk[1]
Institute of Fluid-Flow Machinery, Polish Academy of Sciences
Fiszera 14, 80-231, Gdańsk, Poland
fwasilczuk@imp.gda.pl

Paweł Flaszyński
Institute of Fluid-Flow Machinery, Polish Academy of Sciences
Fiszera 14, 80-9522222, Gdańsk, Poland
pflaszyn@imp.gda.pl

Piotr Doerffer
Gdańsk University of Technology
Narutowicza 11/12, 80-233 Gdańsk Poland
doerffer@imp.gda.pl

Krzysztof Marugi
Avio Polska Sp. z o.o.
Grażyńskiego 141, 43-300, Bielsko-Biała, Poland
krzysztof.marugi@avioaero.it

Tomasz Borzęcki
Avio Polska Sp. z o.o.
Grażyńskiego 141, 43-300, Bielsko-Biała, Poland
tomasz.borzecki@avioaero.it

[1] Corresponding author.

ABSTRACT

This paper presents a study conducted on a new gas turbine, designed to limit leakage in the labyrinth seal. The slots in the fin are used to generate a bypass flow, which obstructs the flow in the gap above the fin. The method was tested numerically and experimentally beforehand using a simplified model without rotation or blade passages. In this paper, the validation of the method using a model of a turbine stage is shown. RANS simulations using two turbulence models – Spalart-Allmaras (SA) and k-ω EARSM were conducted. Comparisons of leakage flow and stage efficiency for reference and fluidic sealing configurations are presented. Fluidic sealing configuration is effective and reduces the leakage flow by 13-18.5% (depending on the turbulence model). The analysis of the flow structure in the seal region revealed, that the use of fluidic sealing resulted in significant circumferential flow anisotropy.

Keywords: Labyrinth Seal, Flow Control, Leakage reduction

1. INTRODUCTION

Pollution from air travel can be reduced by increasing engine efficiency, which also improves operation profitability. There are many aspects of engine operation that can be investigated in order to reduce loss. However, this study is mainly focused on losses resulting from leakage, which contribute up to 25% of stage losses [1]. Seal leakage impacts three aspects of turbine performance. Firstly, it reduces working potential, as some of the air that could work in the blade passage passes through the seal. Secondly, the flow's kinetic energy is dissipated as mixing occurs in the seal. Lastly, the fluid passing through the seal has a different velocity to the fluid in the main channel, thus mixing occurs, leading to decreased performance in further turbine stages [2]. In the shrouded blades, which are investigated in this work, labyrinth seals are used to limit the leakage [3]. Labyrinth seals consist of several fins, which engage in a series of contractions that obstruct the flow. The shape of those fins is optimized to reduce the leakage [4]. Introducing flow control in the seal region can lead to a further reduction, as shown in [5-8]. Considering the widespread use of the gas turbines in aircraft, even a modest reduction in leakage would have a considerable impact globally.

Fluidic sealing in turbine labyrinth seals was first presented in the 1950s patent by Auyer [9], which used pressurized air from a compressor and injected it into the tip gap of an unshrouded turbine. Smile and Paulson [10] implemented the same concept with high pressure air introduced in the cavern between the fins' labyrinth seal of a shrouded blade. Hilfer [11] optimized the configuration, which resulted in a 28% leakage reduction. Placing the fluidic seal in the gap above the fin of the labyrinth seal was first proposed by Rushton [12].

Subsequent research shows passive configurations of the fluidic sealing, where no additional air supply is needed. In this case, the source of pressurized air is usually upstream of the seal [7], where the pressure is greater than in the gap. Ghaffari [13,14] presented a similar idea, but used the elevated pressure from the stagnation point at the leading edge of the turbine blade.

The solution presented in this paper combines two important features of the solutions presented in the literature review, which, to the best of the authors' knowledge, has not been done before. Namely, the bypass slot is entirely incorporated within the fin of the seal while at the same time being passive. The modus operandi is shown in Fig. 1. In the labyrinth seal, the pressure upstream of the fin is higher than downstream of the fin. Therefore, the pressure is higher at the slot inlet than the slot outlet, which drives the flow through the slot. The proposed method is passive, which is an advantage and may lead to an overall improvement in performance in the gas turbine stage.

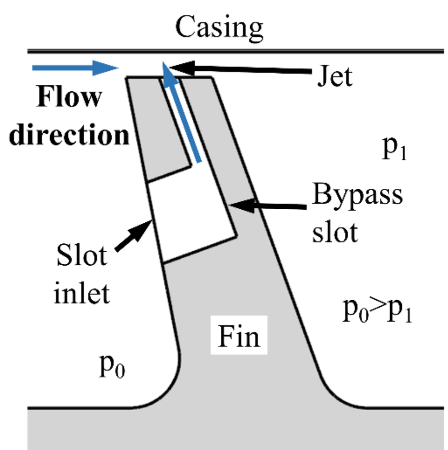

Fig. 1 Operation principle of the fluidic seal [15]

The experiment was conducted on a simplified, static (non-rotating), linear labyrinth seal configuration of a low-pressure turbine stage [5,6,15], where various configurations of the seal were placed in a wind tunnel. The pressure ratio between the section's inlet and outlet was set using valves, after which the stagnation parameters, mass flow at the inlet and pressure distribution in the seal were measured. A pressure ratio ranging from 1.05 to 2.05 was tested to verify the design in a wide range of conditions. One of the selected conditions corresponds to the pressure ratio in the design point of the labyrinth seal in a turbine. However, due to experimental restrictions, the ambient temperature was used instead of the elevated one. Additionally, the test section allowed for the investigation of configurations with different gap heights, which reflects the changing gap height present during turbine operation. However, in this paper only two gap heights are presented: h=0.85s and 1.25s, where s is the thickness of the reference fin.

The experimental results, comparing the reference case and the case with fluidic sealing [5,6] show the leakage reduction of up to 16% was achieved in the latter configuration.

As the purpose of this paper is to present turbine stage simulations, the experimental data is shown only as a validation tool for the numerical model, thus not many details are presented. A more inquisitive reader should refer to [5,6,15], where more information, including the equipment used and measurement errors are presented.

The numerical simulations were carried out using the k-ω EARSM [16] and Spalart-Allmaras [17] turbulence models. Both models showed satisfactory qualitative agreement with the experimental data, with small quantitative differences [5,6]. The efficiency of the fluidic sealing in reducing the leakage flow was proven in simulations using both turbulence models. The CFD approach also showed that fluidic sealing may reduce the leakage flow by up to 22%.

Results from the RANS simulations of simplified configuration (described in detail in section 2) served as a source for a brief description of operating principles of the fluidic sealing presented below. The air at the slot outlet has significant velocity, perpendicular to the main flow, which constitutes an obstacle for the main flow. In addition, the difference in the magnitude and direction of the velocity creates additional vortex structures (Fig. 2), which are described in sections 4 and 6. Additionally, since the slot does not cover the entire fin in the circumferential direction, the main flow is impacted by the flow exiting the slot differently at various sections of the gap. This introduces an additional non-uniformity of the flow in the gap, which then propagates into the cavern between the fins. The non-uniformity causes additional mixing in this zone, which leads to a higher dissipation of kinetic energy in the flow. The comparison of the flow structure with and without the fluidic sealing is analyzed in detail in [6].

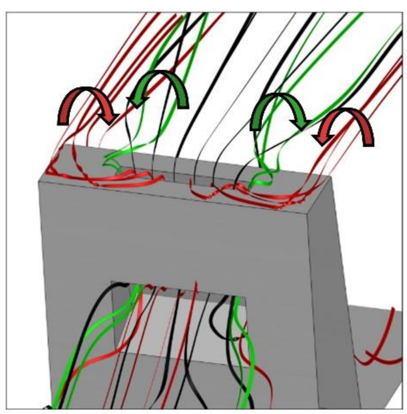

Fig. 2 The vortex structure generated by the fluidic seal, direction of vortex rotation marked with arrows. Example representation based on data obtained in RANS simulations [6].

2. NUMERICAL MODEL VALIDATION

Before fluidic sealing was implemented in the simulations of the turbine stage model, an extensive study was conducted on the simplified model, which included experimental campaign. The comparison of experimental and numerical results was used to validate the numerical model. The definition of the configuration is presented in this section, along the validation results.

Fine/Turbo Numeca code was used to simulate the flow through the labyrinth seal. Steady RANS calculations were conducted, with the k-ω EARSM and Spalart-Allmaras turbulence models. Perfect gas was assumed with viscosity calculated according to Sutherland's law. The code uses the second order central difference spatial discretization scheme with artificial dissipation, as well as the explicit Runge-Kutta numerical scheme. Additionally, the Full Approximation Storage multigrid strategy, with coarse grid initialization was utilized. Numerical settings are presented in Tab. 1.

Tab. 1 Numerical settings for performed simulations.

Parameter	**Setting**
Turbulence model	S-A, EARSM
Spatial discretization	2nd order central difference with artificial dissipation
Numerical scheme	Explicit Runge-Kutta
Multigrid strategy	Full Approximation Storage (3 levels)
Medium	Perfect gas
Viscosity	According to Sutherland law

The boundary conditions were set according to the measurement set up (described in section 1). The stagnation pressure and temperature were set at the inlet and the static pressure at the outlet. Walls were set as adiabatic. The turbulence at the inlet was not measured in the experiment, so it was assumed. The turbulent viscosity ratio was set to 5 and the turbulence intensity to 5%. The configuration has significant contraction (10:1) between the inlet and the channel leading to the labyrinth seal (which is the focus of the study), followed by yet another contraction (about 10:1, depending on gap height) between the channel and the gap above the fin. Thus the turbulence at the inlet does not impact the flow in the seal in meaningful manner.

A block-structured hexahedral mesh was used, refined close to the wall to keep y+ at less than 2 around the seal. The selection of the final grid was preceded by a grid convergence study, so that the results are grid-independent [6]. The final grid size is equal to 5.8 million cells.

The focus of the research presented in this paper is the fluidic sealing, which is created using the slots drilled in the labyrinth seal fins. The crucial geometrical features of the slot such as its outlet dimensions are the same for simplified configuration and stage configuration (shown in sections 4-6). The shape of the slot is a compromise between its effectiveness and the manufacturing feasibility. However, in the future, additive manufacturing technology will allow for more complex and optimal slot shapes. The dimensions of the slot, including the inlet and outlet dimensions as well as the slot inclination angle were determined using a parametric study, presented in [8], while the relative dimensions of the slot are shown in Fig. 3.

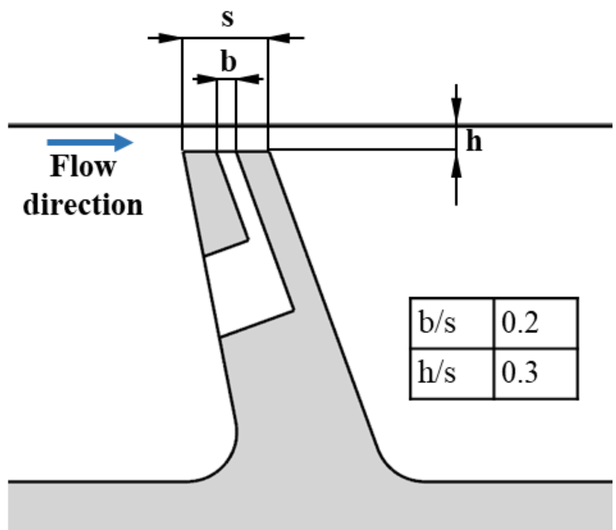

Fig. 3. Geometry of the fluidic sealing slot.

The labyrinth seal configuration was modified to allow for the design of a relatively simple test section, without sacrificing the key features of the seal flow. The simplifications neglect some secondary geometrical features, reducing the model domain to the seal only (without the blade channel) as well as disregarding rotational effects. The analysis of the impact of those simplifications is described extensively in [5]. Overall, it can be concluded, that while some of the simplifications have a non-negligible impact on the level of leakage flow, the main features of the labyrinth seal flow are conserved in the simplified model. Thus, the simplified model was deemed sufficient for proving the concept and assessing the effectiveness of proposed modifications. Nevertheless, testing of the fluidic sealing in the actual turbine configuration before it can be implemented is essential.

Figure 4 presents a comparison of the mass flow from the numerical model with the measurements in the test section, normalized by the maximum value obtained in the experiment. The mass flow for both turbulence models is very similar and is underestimated by about 8% in the entire range. However, the trend of mass flow change with rising pressure ratio is the same for experimental and numerical results. At the same time, the pressure distribution at the platform (upper wall of the model) calculated using both turbulence models, concurs well with the measured values. In previous studies [5,6] it was established, that the leakage flow is sensitive to the turbulence model used. The leakage flow highly depends on the flow area in the gap, which in turn is impacted by separation bubble height. After exiting the gap the flow enters the cavern, where it is also separated. It is well known, that the accuracy of the turbulence models in separated flow is limited. In this case, the proposed model is considered accurate for the purpose of the study. The improvement of accuracy may be obtained with LES simulations, which are planned in the future.

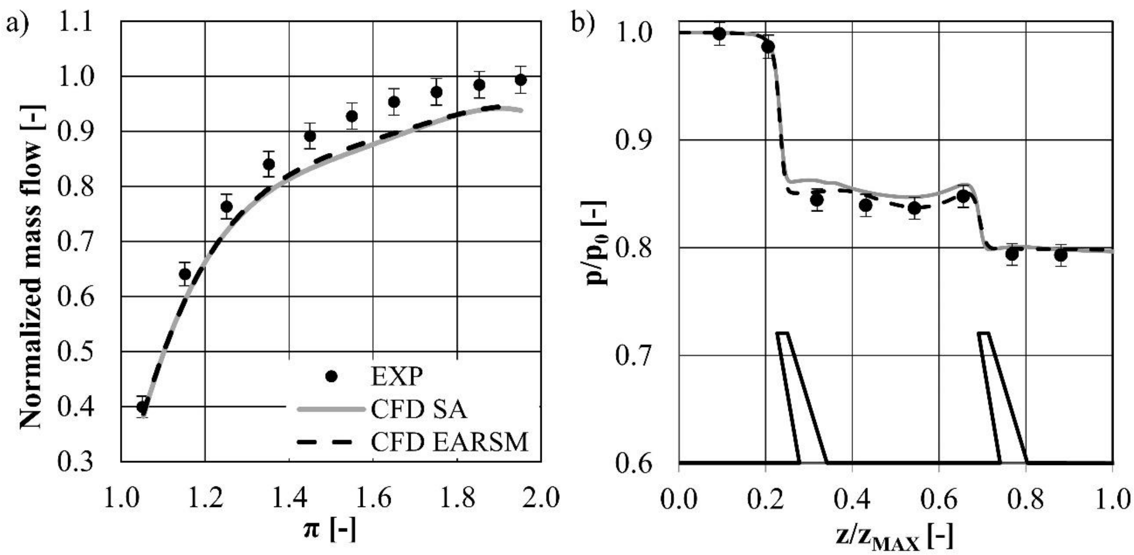

Fig. 4. Comparison of the quantities obtained in the experiment [5] and the numerical model with two turbulence models (Spalart-Allmaras and k-ω EARSM). Gap height = 0.85*s*, pressure ratio = 1.25. a) Mass flow through the seal normalized with the maximum value in the experiment. b) Static pressure at the casing normalized by inlet total pressure.

3. TURBINE STAGE MODEL DESCRIPTION

Turbine stage simulations used the same numerical settings as the simplified configurations simulations, while the geometry and boundary conditions were modified.

The details of the seal configuration are protected, but key information can be shared. Similarly to the configuration used in the experimental step, the seal in the stage configuration has two fins, the clearance used was 0.38 of the fin thickness. However, there are some geometrical differences between the simplified (experimental) and the stage configuration, due to the labyrinth seal optimization conducted in the period between the experiment and the stage simulations [18]. Figure 5 presents comparison of two configurations – simplified and stage. Apart from geometry differences, other differences between the models that were mentioned in section 2 and discussed in detail in [5] are listed in the figure.

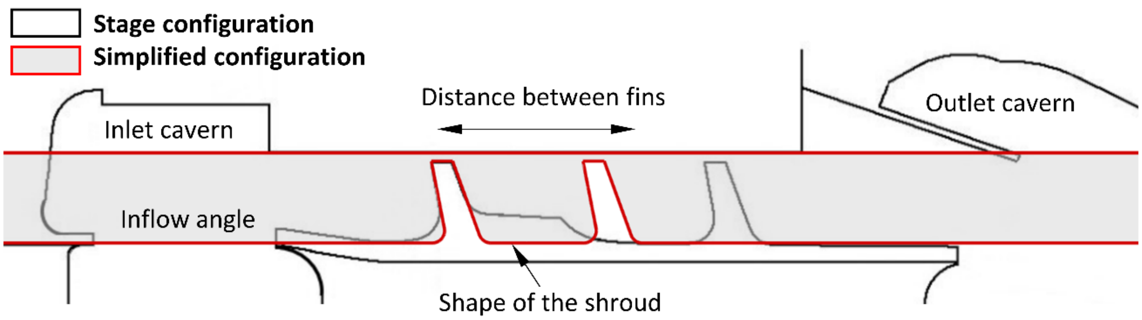

Fig. 5. Schematic comparison of stage and simplified configurations. Differences between configurations are listed in the figure.

Even though the stage configuration is much more faithful representation of a real turbine than the simplified configuration, there is one major difference between it and the real engine – namely the honeycomb at the casing was neglected. The experimental studies on the simplified test section show that the currently investigated fluidic sealing is not effective when a honeycomb is used. This issue is still being researched, as the honeycomb adds complexity to the case. Some of the concepts that can make the configuration with fluidic sealing and the honeycomb combination effective are discussed in [15]. It is important to note, that the fluidic sealing is investigated as a means to reduce the leakage flow in a wide range of applications, where the clearance is small and unavoidable, not only in LP turbines, where honeycombs are prevalent.

The stage used in simulations is defined based on the last stage of a low-pressure turbine of a GEnx engine. As with the seal geometry, the details cannot be shown, but for reference approximate dimensions and features are specified below. The stator consists of 168 blades, while the rotor of 114 blades. The shroud radius is about 1 m, with blades length of about 300 mm. The gap between the casing and the labyrinth seal roughly 1 mm. The rotation rate of the rotor is 2100 RPM. The ratio of total pressure ratio at stage inlet and static pressure at the outlet is equal to 1.6.

Two models were created with two versions of the labyrinth seal mounted on the rotor blade. In the reference configuration a standard, unmodified labyrinth seal was installed, while the seal of the second model included fluidic sealing slots. Apart from the slots, both configurations were identical.

The grid for the blades channel was generated by the Autogrid/Numeca code with O4H topology, which provided good quality [15,19]. The grid of the labyrinth seal (Fig. 6) was created in IGG/Numeca and added to the channel grid. The grid of the labyrinth seal was split into two parts, one connected to the stator grid and the one to the rotor grid (see Fig. 7). The periodicity of the seal grid matches the periodicity of the blade passage. Both domains - the seal and the blade passage, were connected with non-matching interfaces. The non-matching connection is created using Alternating Digital Trees (ADT) algorithm [20]. One side of the connection is triangulated and projected on the other side.

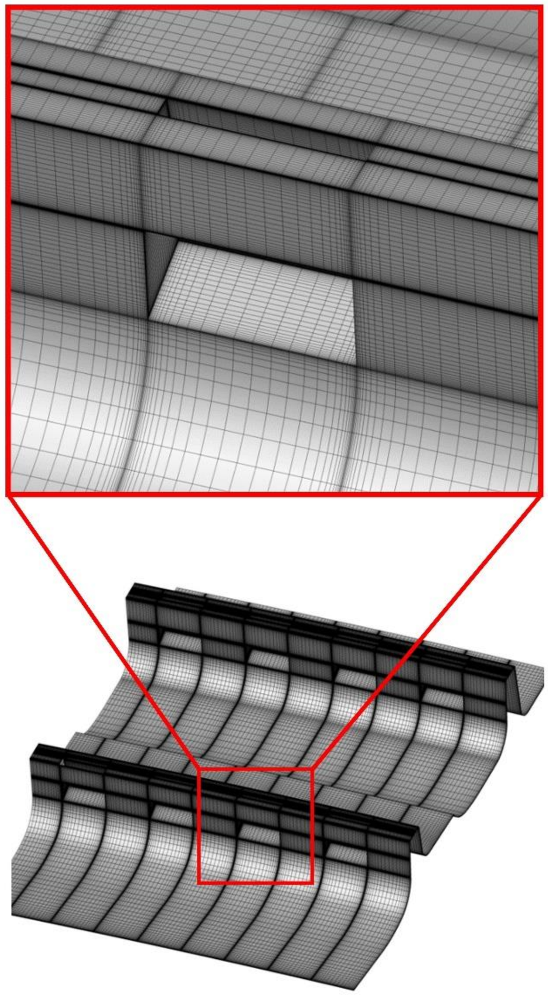

Fig. 6. Grid of the labyrinth seal.

The grid resolving the flow through the blades consists of two parts – rotor part and stator part, connected with rotor-stator interface. Table 2 shows the grid resolution in selected directions, such as radial, circumferential, pressure side (PS) and suction side (SS) resolution for the blades, as well as resolution in all three directions for the seal and the gap above the fin.

Tab. 2 Resolution of the computational grid in selected directions

	Circumferential (X)	Radial (Y)	Axial (Z)	
Gap	364	36	112	
Seal	364	128	412	
Stator	64	108	112 (PS)	232 (SS)
Rotor	125	108	116 (PS)	300 (SS)

Appropriate grid resolution on the side walls of the slot leads to a significant number of elements in the circumferential direction. This causes the grid to be large. Introducing a non-matching interface (Fig. 7) allows for the reduction of circumferential resolution in the inlet and outlet caverns of the seal, where refinement is not required. As a result, the mesh size can be significantly reduced. Still, the final grid consists of 21 million cells, out of which about 16.5 million are located in the labyrinth seal zone.

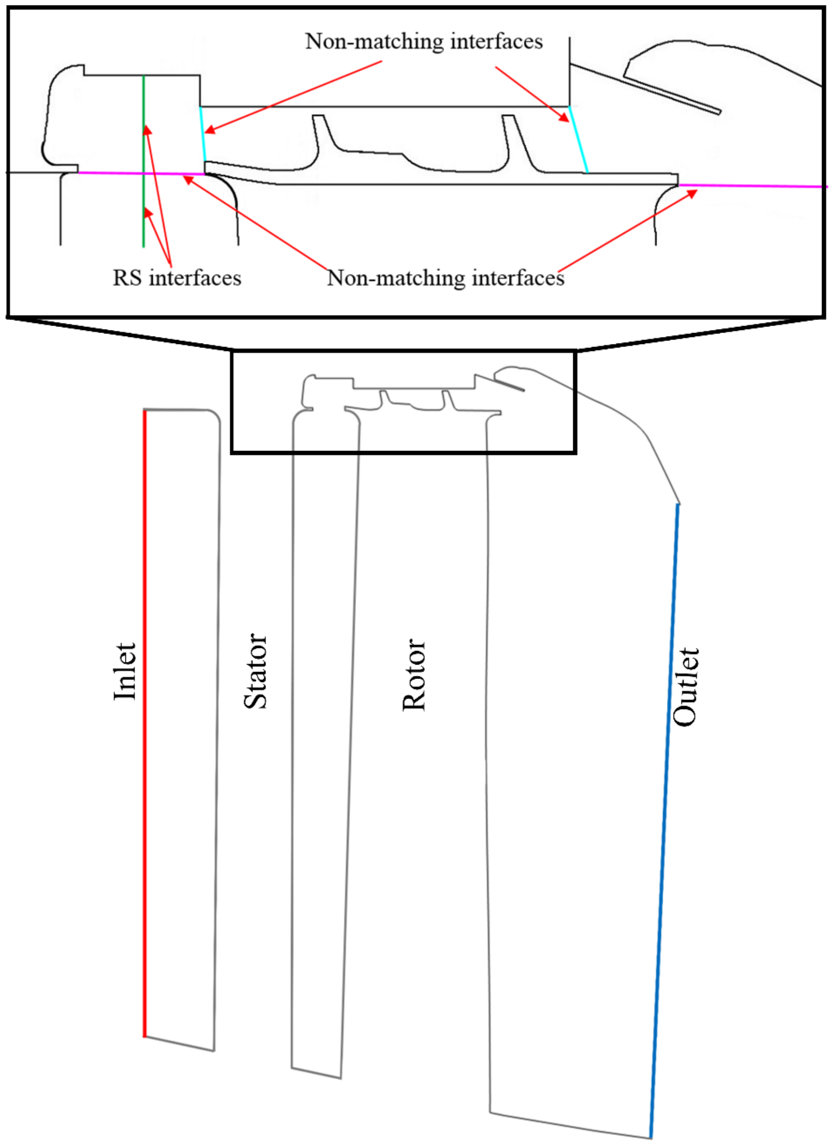

259

260 Fig. 7. A numerical model of a turbine stage with the labyrinth seal, with marked

261 boundary conditions and interfaces used.

262

The boundary conditions were a result of a 2D, throughflow simulation of the entire engine. The distribution along the turbine radius of total pressure p_1 (average ~60 kPa), temperature T_1 (average ~700K) and flow direction was specified at the inlet, upstream of the stator. Turbulence quantities were not known, therefore they were assumed: the turbulent viscosity ratio was at 10 and turbulence intensity at 5%. However, the turbulence quantities at the inlet should not impact the flow in the labyrinth seal, since before reaching it, the flow passes through the turbine stator. At the outlet, a static pressure level of 38 kPa was imposed at the radius of the hub with the hub-to-shroud pressure profile calculated according to the radial equilibrium conditions [21]. The speed of rotation is 2100 RPM.

As for the simplified seal configuration the Numeca/FineTurbo code, which is widely used for turbomachinery simulations, was applied. Simulations were carried out for the steady flow and the full non-matching mixing plane (with the conservation of fluxes) for stator/rotor interface. Additionally, the field variables on one side of the interface were circumferentially averaged and applied to the other side.

4. TURBINE STAGE MODEL COMPARED TO SIMPLIFIED CONFIGURATION

As mentioned before, the concept of fluidic sealing in a turbine labyrinth seal was proved effective for simplified, non-rotating configurations. However, due to the simplifications used in the model, additional simulations with fluidic sealing applied to a turbine stage configuration were performed. This made it possible to check the concept in target conditions.

Ideally, the numerical model for the turbine stage with the labyrinth seal would be validated against the experimental data. However, even conducting the experiment with just the rotating labyrinth seal (without the blade channel) would be too complex a task and currently beyond available options. Therefore, despite the number of differences between the simplified case and the turbine stage configuration, a qualitative comparison is presented to show that the main features of the labyrinth seal and fluidic sealing flow characteristics are maintained. The differences between cases include (Fig. 5):

- Geometry
- Rotational velocity
- Boundary conditions

Obviously, the simplified case (the static test section) did not include rotational velocity, which is present in stage simulations. While the absolute-to-static pressure ratio differs between the cases (due to the significant dynamic pressure from rotational velocity), the static-to-static pressure ratio in the seal is the same for both cases (the dynamic pressure from axial velocity at the seal inlet is negligible). It is worth noticing, that in the stage simulations, the pressure ratio in the seal is not prescribed, but rather a result of the blade passage solution. The rotational velocity in the seal is significant for the stage simulations, while for the experimental setup it is non-existent. Moreover, in the simplified case, an ambient temperature was set, while in the stage simulations the inlet temperature was derived from the real turbine.

Because of these differences, a direct comparison of the mass flows obtained in the experiment and the stage simulations is not valid. Instead, a qualitative comparison of the flow structure created by the jet exiting the fluidic sealing slot, is shown in the following section. The axial velocity profiles (normalized with the maximum value) at two traverses located at the outlet of the gap above the fin are presented in Fig. 8. The first traverse is located in the middle of the slot (black lines) and the second one between the neighboring slots (grey lines). While the flow structure for the stage configuration will be investigated in more detail in section 6, it is worth noting the similarities and differences between the stage and experimental configurations. In both cases, the average velocity is greater in the area between the slots than in the zone where the jet exits the slot, causing a velocity reduction. In the space in the gap close to the slot, the velocity field is very similar in both cases. Downstream of the gap, the flow in the stage configuration is subject to rotational effects (discussed in more detail below), thus differences arise. In both cases, in the area between the slots, the separation in the gap which is present in the reference configurations (not shown here), is reduced when fluidic sealing is used. In the stage configuration, the velocity is almost constant across the gap (excluding the boundary layers), while in the experimental configuration it is variable. This happens, because the complex vortical structure generated by the jet in the simplified configuration is disturbed by significant rotational velocity.

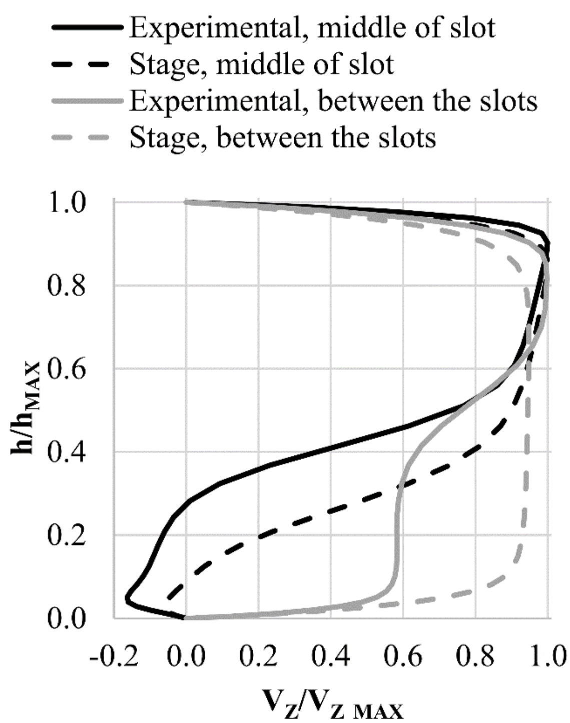

Fig. 8. Profile of the normalized axial velocity in the first gap for two traverses in the experimental and stage configurations.

Fig. 9 presents the streamlines of relative velocity. The jet exiting the slot (black streamlines) creates a fluidic seal, that obstructs the main flow. Additionally, the air exiting the slot in a sideways direction generates stream-wise vortices. They are present in both of the configurations shown, however in the stage configuration the vortices are much less developed and more thinly spread in the circumferential direction. In the simplified configuration one can also notice that the air exiting from the front part of the slot (red streamlines) enters the separation vortex and later forms a counter-rotating vortex in the area between the slots. This flow feature is not present in the stage configurations, as the separation is less pronounced due to the significant rotation velocity of the fin. Moreover, the flow structures generated by mass transport in the tangential direction are subject to disturbance caused by the rotational velocity of the fin.

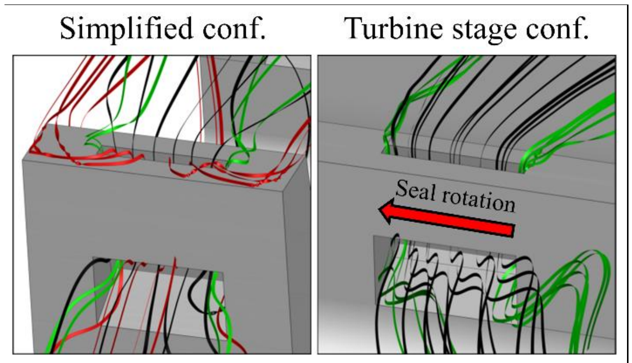

Fig. 9. Comparison of vortex structure in experimental and stage configurations.

Overall, some of the flow features, such as velocity reduction in the area of the slot and the generation of streamwise vortices at the side edges of the slot, are similar in both presented configurations. The flow in the area between the slots has a higher average velocity in both configurations, however the velocity profile in the gap differs. Additionally, the counter rotating vortices in the area between the slots are not present in the stage configuration, contrary to the experimental configuration.

5. TURBINE STAGE MODEL RESULTS

The investigation of the impact of fluidic sealing on the flow through a labyrinth seal in the turbine stage is split into two parts. Firstly, the change in global parameters, such as leakage flow and stage efficiency is presented. This is followed by a comparison of the flow structure existing in the reference case and the case with the fluidic seal. This is helpful in assessing the reasons for the change in the global parameters.

The implementation of fluidic sealing in the labyrinth seal of a turbine stage reduces the leakage flow. The predicted reduction depends on the turbulence model used in the simulation. For k-ω EARSM it is equal to 13%, while for Spalart Allmaras it is 18.5% (Fig. 10). This difference is caused by different separation sizes in the gap above the fin, predicted by these models, which is discussed in the next paragraph. Interestingly, the reduction of the leakage flow leads to a slight increase in the blade passage flow.

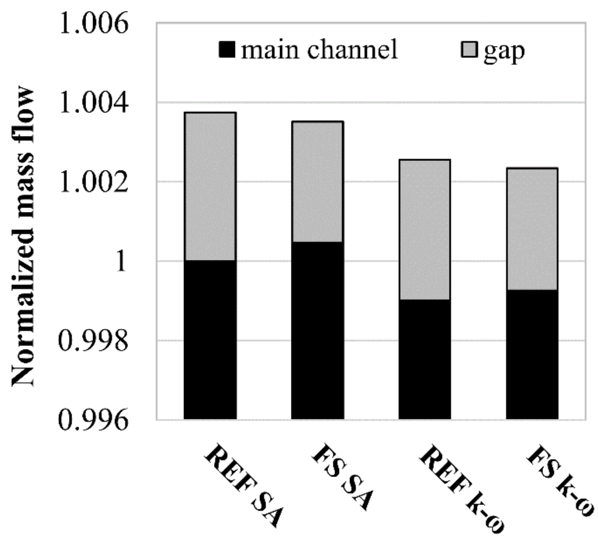

Fig. 10. Mass flow for reference and fluidic seal configuration, normalized with the value of main channel flow for reference Spalart Allmaras case.

Decreasing leakage leads to an increase in stage isentropic total to total efficiency, which is defined as:

$$\eta = \frac{1 - \frac{T_2}{T_1}}{1 - \left(\frac{p_2}{p_1}\right)^{\frac{\kappa - 1}{\kappa}}} \tag{1}$$

Where:

p_1, p_2 – total pressure at inlet and outlet

T_1, T_2 – total temperature at inlet and outlet

κ – heat capacity ratio

Of course, the isentropic efficiency increase is also dependent on the turbulence model and is equal to 0.065% and 0.04% for k-ω EARSM and Spalart-Allmaras respectively. This efficiency increase is not large, however there are several reasons why the concept is worth further investigation. Firstly, in the case of the investigated stage, the blades are very long compared to the gap size, so the leakage flow is only 0.3% of the total mass flow. Therefore, even a significant leakage reduction impacts the stage efficiency only marginally. In the future, the concept will be tested further using blades with different lengths. Additionally, the slots that generate fluidic sealing were not optimized to operate in the rotating framework. In fact, as the aim of the research was to test the viability of the fluidic sealing as a leakage reduction device, the geometry of the slot was not optimized. Last but not least, the presented efficiency is calculated for one stage only, implementing fluidic sealing in more stages would likely bring further gains, since the leakage would be reduced at each stage. Leakage losses are not only connected with loss of working potential, which is could be treated as isolated to the single stage, but also the mixing losses that impact other stages.

6. FLOW FIELD ANALYSIS

A flow field analysis was conducted to study the reason behind the leakage reduction when the fluidic sealing was used. A comparison of the flow structure in the reference and the fluidic sealing cases is presented in Figs. 11-12. Figure 11 shows the contour of the axial velocity in the meridional cross-section. Even though there is some circumferential non-uniformity in the reference case, it is minor in comparison to the fluidic sealing case. Therefore, only one cross-section for the reference case is shown, while for the fluidic sealing case, the cross-sections in the middle of the slot as well as in the area between the slots are shown. In Fig. 12, the axial velocity distribution in the constant radius surface is shown. This surface is located in the middle of the tip gap. The location of the fins and slots (in the fluidic sealing case), as well as the rotation direction, is marked in the figure. In the cross section, recirculation zones with very low velocity in the cavities upstream and downstream of the seal can be noticed.

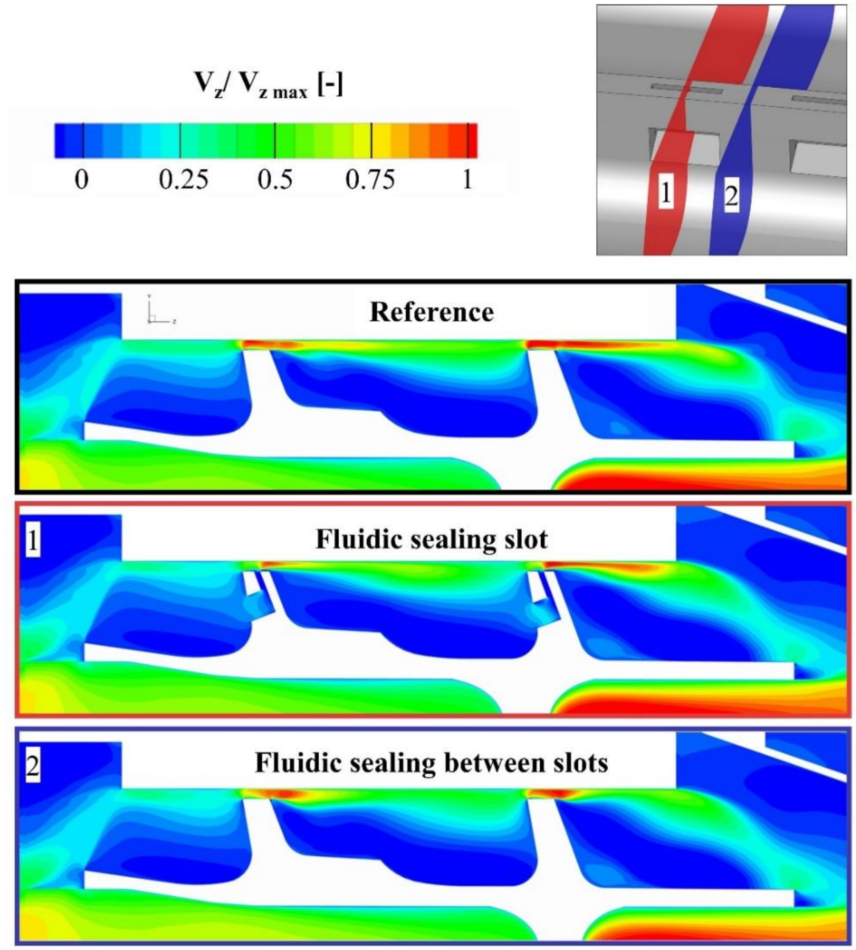

Fig. 11. Normalized axial velocity for the reference case and the two cross-sections of the fluidic sealing case.

In the reference case, the flow accelerates in the gaps above the fins. This leads to the creation of the high velocity zone that goes into the area between the fins (which can be seen in Fig. 11). A similar zone is created above the second fin. In Fig. 12, the non-uniformity of velocity in the circumferential direction can be noticed. The flow through the blade passages is not uniform, which impacts the conditions at the inlet and outlet of the seal. Additionally, the slight impact of the computational grid can be noticed. As mentioned before, both the reference and fluidic sealing grids are very similar, with the only difference being the presence of slots. In the fluidic sealing case, the grid was created so that the boundary layer inside the slots was properly resolved. This means that the grid refinements which are close to walls propagate in an axial direction which causes visible non-uniformity in the circumferential direction. This effect also exists in the reference grid, since both grids are almost the same. Nevertheless, the non-uniformity of the flow in the reference case, resulting from the grid resolution, is minor and does not significantly affect the results. In fluidic sealing case, the periodic high velocity zones downstream of the second fin have a different periodicity than the grid blocks.

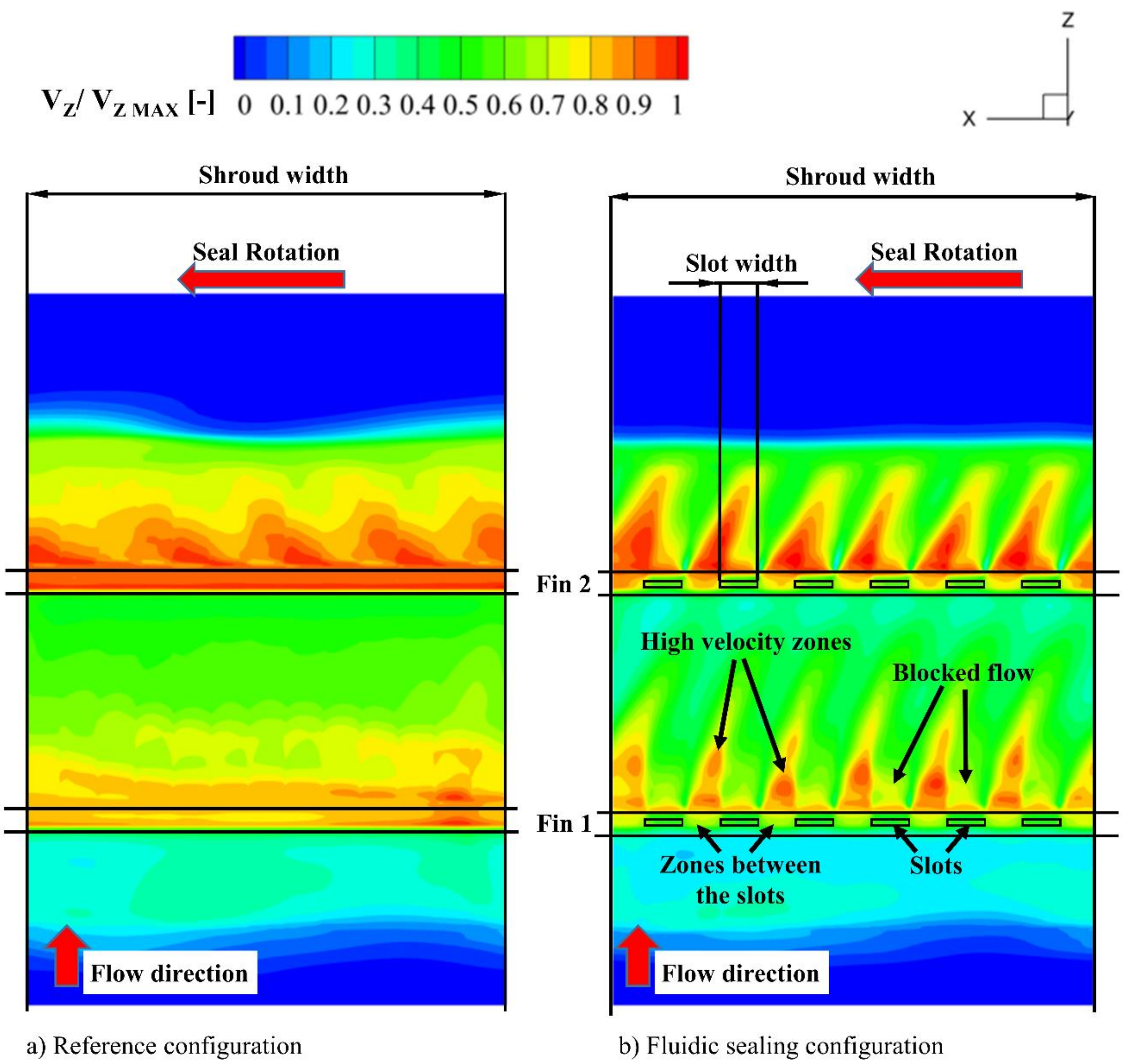

Fig. 12. Normalized axial velocity for the reference and the fluidic sealing case for a constant radius cross-section.

Implementing fluidic sealing significantly impacts the flow in the gap above the fins. Strong circumferential non-uniformity is present, with two distinct flow patterns. Firstly, in the zones above the slots, the high velocity is significantly diminished in comparison with the reference case. The main flow in that region is blocked and pushed upwards by the jet exiting the slots. Moreover, the very presence of the jet causes the expansion of the high velocity zone in the cavern to be less prevalent than in the reference case (Fig. 11, cross section 1).

On the other hand, a part of the flow blocked by the jets exiting the slots, passes the gap through the zone between the slots. This increases the maximum velocity there and the size of the high velocity zone (Fig. 11, cross section 2). In contrast to the zone above the slots, the flow exiting the gap between the slots expands more in the cavern than in the reference case. One can easily notice in Fig. 12, that the high velocity zones created between the slots, enter the cavern between the fins and bend in the opposite direction to the rotation. This is a result of rotation. The circumferential velocity component in the gap is almost equal to the rotation velocity of the seal, therefore, the shape of the high velocity zones in the gap is not changed. At the same time, the circumferential velocity in the cavern, between the fins and downstream of the second fin is lower than the rotation velocity of the seal. Thus, in the rotating frame of reference, the high velocity zone seemingly bends in the opposite direction to the rotation.

In addition, the velocity exiting the seal is slightly more uniform than in the reference case. This is caused by increased mixing due to the high non-uniformity of the flow in the circumferential direction. A more uniform flow at the outlet may be beneficial since mixing occurs between the flow exiting the seal and the blade passage flow. However, this aspect should be further investigated.

In the non-rotating framework, the air exits the slots in a direction which is aligned with the main flow, but also with the sides of the slot. When the seal rotates, it has an additional circumferential component. The superposition of those two effects results in non-symmetric flow in the gap, which can be observed in Fig. 13. On the one side of the slot, where the direction of the velocity exiting the slot matches that of the circumferential velocity, there is a local speed-up. On the opposite side of the slot, the circumferential velocity is reduced by the velocity of the flow exiting the slot. This promotes additional mixing and may be one of the reasons for more overall flow uniformity at the exit of the seal.

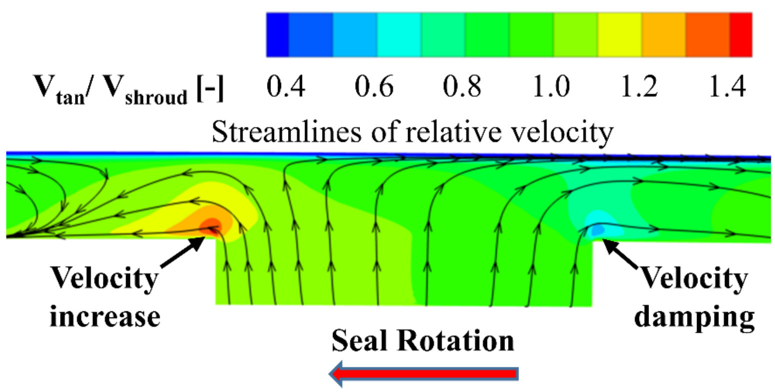

Fig. 13. Contour of circumferential velocity, normalized by the velocity of shroud rotation. Streamlines (in plane) in rotating frame.

7. CONCLUSIONS

This new concept for fluidic sealing in labyrinth seals, which was previously tested only in simplified conditions, was implemented in turbine stage simulations. As in the simplified configurations shown in [5,6], the fluidic sealing proved to be effective in reducing the leakage flow. The reduction predicted by the simulations differs, depending on the turbulence model used, with 18.5% reduction obtained for Spalart Allmaras and 13% for k-ω EARSM. Evaluation of the stage isentropic efficiency shows improvement by 0.065% and 0.04% for k-ω EARSM and Spalart-Allmaras.

The flow structure in the reference and fluidic sealing configurations was compared. The comparison revealed that the jet exiting the slots blocks the flow and leads to significant circumferential flow non-uniformity. This promotes mixing, which in turn increases flow resistance, eventually leading to a decrease in leakage flow.

8. FURTHER WORK

Since the fluidic sealing concept has proven to be viable, further steps can be taken in order to assess its full potential, as well as to tackle possible implementation challenges.

Firstly, the shape of the fluidic sealing slot used in this study was not optimized with rotating machinery in mind. Therefore, the concept could be more efficient if the slots were a different shape and were inclined in a circumferential direction.

The leakage reduction and stage efficiency gain resulting from the use of fluidic sealing should be also assessed for different stages of the turbine and shorter blades. Such a study would show whether the gains achieved in the entire turbine are significant enough to warrant further investigation.

Additional analyses, regarding material strength and possible manufacturing techniques should be performed. This would allow for a more precise selection of optimization constraints for the slot. This may also lead to an improvement in efficiency.

Last but not least, an experimental campaign using a rotating seal could be conducted to validate the numerical model in a more robust manner. This would definitely illustrate whether or not the concept is viable in rotating seals.

9. ACKNOWLEDGMENT

This research was supported by CI TASK and by PL-Grid Infrastructure in part.

10. FUNDING

This work was supported by the Coopernik project “Cooperative Research for Next Generation High Efficiency LP Turbine” INNOLOT/I/11/NCBR/2014.

11. NOMENCLATURE

b	Size of the slot in axial dimension
h	Gap height
p	Pressure
p_1	total pressure at inlet
p_2	total pressure at outlet
T_1	total temperature at inlet
T_2	total temperature at outlet
s	Thickness of the fin of the seal
$y+$	Non dimensional wall distance
V_{tan}	Tangential velocity
V_{shroud}	Velocity of the shroud
V_Z	Axial velocity
z	Axial dimension
κ	heat capacity ratio
π	Inlet to outlet pressure ratio
CFD	Computational Fluid Dynamics
FS	Fluidic Sealing
HP	High pressure
k-ω EARSM	k-ω Explicit Algebraic Reynolds Stress turbulence model
LP	Low pressure
PS	Pressure side
RANS	Reynolds Averaged Navier Stokes
REF	Reference case (without modifications)
RPM	Revolutions per minute

RS	Rotor-Stator
SA	Spalart-Allmaras turbulence model
SS	Suction side

12. REFERENCES

[1] Pfau, A., 2003, “Loss Mechanisms in Labyrinth Seals of Shrouded Axial Turbines”, PhD Dissertation, ETH Zurich, Zurich, Switzerland.

[2] Kim S., Kim K., Son C., 2019 “Three-dimensional unsteady simulation of a multistage axial compressor with labyrinth seals and its effects on overall performance and flow characteristics”, *Aerospace Science and Technology,* 86 (2019), pp. 683-693, DOI: https://doi.org/10.1016/j.ast.2019.01.055.

[3] Denton J.D., 1993, “Loss mechanisms in turbomachines, *ASME J. Turbomach*. 115(4) (1993) 621, https://doi.org /10.1115 /1.2929299.

[4] Lin, Z., Wang, X., Yuan, X.,. Shibukawa N., Noguchi T., 2015, “Investigation and improvement of the staggered labyrinth seal” *Chin. J. Mech. Eng*. 28 (2), pp. 402-408, https://doi.org/10.3901.

[5] Wasilczuk F., Flaszyński P., Kaczyński P., Szwaba R., Doerffer P., Marugi K., 2021 “Air curtain application for leakage reduction in gas turbine shroud sealing”, *Aeropace Science and Technology*, 112, https://doi.org/10.1016/j.ast.2021.106636

[6] Wasilczuk F., Flaszyński P., Kaczyński P., Szwaba R., Doerffer P., Marugi K., 2021, “Passive Reduction of Leakage by Transverse Jet”, *J Fluids Eng – Transactions of the ASME*, 143

[7] Turnquist, N. A., Bruce, K. L., Cerretelli, C., Tourigny J. E., 2009, “Fluidic sealing for turbomachinery”, US patent No. 8052375B2, USA.

[8] Wasilczuk, F., Flaszynski P., Pyclik L., and Marugi K., 2021, "Feasibility Study of Fluidic Sealing in Turbine Shroud" *Materials,* 14, no. 13: 3477. https://doi.org/10.3390/ma14133477

[9] Auyer, E. L., 1954, “Dynamic sealing arrangement for turbomachines,” US patent No. 2,685,429, USA.

[10] Smile, H. J. and Paulson E. E., 1960, “Pressurized seal,” US patent No. 2963268, USA.

[11] Hilfer M., Hogg S., Ingram G., 2015, “Experimental Validation of a Curtain Type Fluidic Jet Seal on a Turbine Rotor Shroud,” Proceedings of the ASME Turbo Expo 2015: Turbine Technical Conference and Exposition. Volume 5C: Heat Transfer. Montreal, Quebec, Canada. June 15–19, 2015, ASME Paper No. GT2015-42624, https://doi.org/10.1115/GT2015-42624.

[12] Rushton, G. J., 2007, “Seal arrangement” US patent No. 7238001B2, USA.

[13] Ghaffari, P. and Willinger, R., 2016, "On the Impact of Passive Tip-Injection on the Downstream Flow Field of a Shrouded LP-Turbine: CFD and Experimental Results," Proceedings of the ASME Turbo Expo 2016: Turbomachinery Technical Conference and Exposition. Volume 2B: Turbomachinery, Seoul, South Korea. June 13–17, 2016. ASME Paper No. GT2016-56196, https://doi.org/10.1115/GT2016-56196.

[14] Ghaffari P. and Willinger R., 2015, “Preliminary Investigation of Passive Tip-Injection in a Linear Turbine Cascade.”, ETC Paper No. 205, 11th European Turbomachinery Conference, Madrid, Spain, 2015

[15] Wasilczuk F., 2020, “Fluidic Control of Shroud Leakage Flow in Gas Turbine”, PhD Thesis, IMP PAN, Gdańsk, Poland

[16] Menter F., Garbaruk A., Egorov Y., 2012, "Explicit algebraic Reynolds stress models for anisotropic wall-bounded flows", *Progress in Flight Physics* 3 (2012) 89-104, https://doi.org/10.1051/eucass/201203089

[17] Spalart, P. R. and Allmaras, S. R., 1992, “A one-equation turbulence model for aerodynamic flows”, AIAA 30th Aerospace Sciences Meeting and Exhibit 06 January 1992 - 09 January 1992 Reno, NV, USA, https://doi.org/10.2514/6.1992-439.

[18] Szymański, A., Wróblewski, W., Frączek, D., Bochon, K., Dykas, S., and Marugi, K. 2018 "Optimization of the Straight-Through Labyrinth Seal With a Smooth Land." *ASME J Eng Gas Turbines Power*. December 2018; 140(12): 122503. https://doi.org/10.1115/1.4040767

[19] Numeca, 2014, “Theoretical Manual”, November, Numeca, 2014.

[20] Bonet, J. and Peraire, J. (1991), An alternating digital tree (ADT) algorithm for 3D geometric searching and intersection problems. Int. J. Numer. Meth. Engng., 31: 1-17. https://doi.org/10.1002/nme.1620310102

[21] Wu, C.-H., & Wolfenstein, L., 1950, “Application of radial-equilibrium condition to axial-flow compressor and turbine design.”, NACA Report No. 955

13. Table caption list

Tab. 1 Numerical settings for performed simulations.

Tab. 2 Resolution of the computational grid in selected directions

14. Figure caption list

Fig. 1 Operation principle of the fluidic seal [15]

Fig. 2 The vortex structure generated by the fluidic seal, direction of vortex rotation marked with arrows. Example representation based on data obtained in RANS simulations [6].

Fig. 3. Geometry of the fluidic sealing slot.

Fig. 4. Comparison of the quantities obtained in the experiment [5] and the numerical model with two turbulence models (Spalart-Allmaras and k-ω EARSM). Gap height = 0.85s, pressure ratio = 1.25. a) Mass flow through the seal normalized with the maximum value in the experiment. b) Static pressure at the casing normalized by inlet total pressure.

Fig. 5. Schematic comparison of stage and simplified configurations. Differences between configurations are listed in the figure.

Fig. 6. Grid of the labyrinth seal.

Fig. 7. A numerical model of a turbine stage with the labyrinth seal, with marked boundary conditions and interfaces used.

Fig. 8. Profile of the normalized axial velocity in the first gap for two traverses in the experimental and stage configurations.

Fig. 9. Comparison of vortex structure in experimental and stage configurations.

Fig. 10. Mass flow for reference and fluidic seal configuration, normalized with the value of main channel flow for reference Spalart Allmaras case.

Fig. 11. Normalized axial velocity for the reference case and the two cross-sections of the fluidic sealing case.

Fig. 12. Normalized axial velocity for the reference and the fluidic sealing case for a constant radius cross-section.

Fig. 13. Contour of circumferential velocity, normalized by the velocity of shroud rotation. Streamlines (in plane) in rotating frame.